European Radiology (2019) 29:4228–4238
https://doi.org/10.1007/s00330-018-5928-7

COMPUTED TOMOGRAPHY

Metal artifacts in patients with large dental implants and bridges: combination of metal artifact reduction algorithms and virtual monoenergetic images provides an approach to handle even strongest artifacts

Kai Roman Laukamp[1,2,3] · David Zopfs[1] · Simon Lennartz[1] · Lenhard Pennig[1] · David Maintz[1] · Jan Borggrefe[1] · Nils Große Hokamp[1]

Received: 21 September 2018 / Revised: 6 November 2018 / Accepted: 28 November 2018 / Published online: 16 January 2019

Abstract

Objectives This study compares reduction of strong metal artifacts from large dental implants/bridges using spectral detector CT-derived virtual monoenergetic images (VMI), metal artifact reduction algorithms/reconstructions (MAR), and a combination of both methods (VMI_{MAR}) to conventional CT images (CI).

Methods Forty-one spectral detector CT (SDCT) datasets of patients that obtained additional MAR reconstructions due to strongest artifacts from large oral implants were included. CI, VMI, MAR, and VMI_{MAR} ranging from 70 to 200 keV (10 keV increment) were reconstructed. Objective image analyses were performed ROI-based by measurement of attenuation (HU) and standard deviation in most pronounced hypo-/hyperdense artifacts as well as artifact impaired soft tissue (mouth floor/soft palate). Extent of artifact reduction, diagnostic assessment of soft tissue, and appearance of new artifacts were rated visually by two radiologists.

Results The hypo-/hyperattenuating artifacts showed an increase and decrease of HU values in MAR and VMI_{MAR} (CI/MAR/$VMI_{MAR\text{-}200keV}$: $-369.8 \pm 239.6/-37.3 \pm 109.6/-46.2 \pm 71.0$ HU, $p < 0.001$ and $274.8 \pm 170.2/51.3 \pm 150.8/36.6 \pm 56.0$, $p < 0.001$, respectively). Higher keV values in hyperdense artifacts allowed for additional artifact reduction; however, this trend was not significant. Artifacts in soft tissue were reduced significantly by MAR and VMI_{MAR}. Visually, high-keV VMI, MAR, and VMI_{MAR} reduced artifacts and improved diagnostic assessment of soft tissue. Overcorrection/new artifacts were reported that mostly did not hamper diagnostic assessment. Overall interrater agreement was excellent (ICC = 0.85).

Conclusions In the presence of strong artifacts due to large oral implants, MAR is a powerful mean for artifact reduction. For hyperdense artifacts, MAR should be supplemented by VMI ranging from 140 to 200 keV. This combination yields optimal artifact reduction and improves the diagnostic image assessment in imaging of the head and neck.

Key Points

- *Large oral implants can cause strong artifacts.*
- *MAR is a powerful tool for artifact reduction considering such strong artifacts.*
- *Hyperdense artifact reduction is supplemented by VMI of 140–200 keV from SDCT.*

Keywords Tomography, X-ray computed · Artifacts · Head and neck neoplasms · Neoplasm metastasis

✉ Kai Roman Laukamp
kai.laukamp@uk-koeln.de

[1] Institute for Diagnostic and Interventional Radiology, University Hospital Cologne, Kerpener Straße 62, 50937 Cologne, Germany

[2] Department of Radiology, Case Western Reserve University, Cleveland, OH, USA

[3] Department of Radiology, University Hospitals Medical Center, Cleveland, OH, USA

Abbreviations

CI	Conventional images
MAR	Metal artifact reduction algorithm
SD	Standard deviation
SDCT	Spectral detector CT
VMI	Virtual monoenergetic images
VMI_{MAR}	Combination of virtual monoenergetic images and metal artifact reduction algorithms

Introduction

Computed tomography is broadly used for imaging head and neck pathologies. Of especial interest are the detection and characterization of tumors, including primary tumors of the head and neck region as well as metastases in staging examinations. Injuries that occur in trauma settings, inflammation, and depiction of vascular pathologies are other common reasons for CT imaging; however, in daily practice, these routine examinations are often strongly hampered by artifacts arising from large oral implants. Artifacts from metal implants result for different reasons: (i) absorption of low energy photons resulting in beam hardening artifacts, (ii) complete absorption of photons resulting in photon starvation, and (iii) scatter artifacts resulting from differences in attenuation between highly attenuating implants and soft tissue. The results are interferences that strongly hamper diagnostic evaluation of the surrounding structures, including soft tissue, lymph nodes, vessels, and bone [1–5]. Several parameters can impact severity of artifacts caused by metal implants. Especially, the composition of metal implants is important. Image acquisition and image reconstruction parameters are also factors to be considered [2].

Conventional CT imaging (CI) can address these artifacts by optimization of acquisition protocols and reconstruction parameters, regarding high tube current (mAs) and voltage (kV), precise collimation, larger slice thickness, and reconstruction filters. Nevertheless, increasing tube current and voltage also increases radiation dose for the patient and is therefore not an option for general application [2].

Another approach for reduction of strong artifacts is the usage of dedicated metal artifact reduction algorithms (MAR) which are available from different vendors and generally designed for larger implants and artifacts, respectively [6–9]. In this study, we applied a specialized MAR which uses an iterative loop that subtracts the output correction data from the original input data [6, 7]. So far, MAR have proven to be effective in phantom studies as well as in clinical applications regarding dental implants, total hip replacements and deep brain stimulation electrodes [5, 7, 9–12].

Virtual monoenergetic images (VMI) that are supplied by several dual-energy CT scanners also constitute a useful approach for metal artifact reduction [13–15]. Dual-energy CT detects photons of low and high energies separately and thereby allows for reconstructions of VMI that correspond to images resulting from true monoenergetic x-ray examinations. Among others, VMI at higher keV values are more resistant against beam hardening and thereby reduce metal artifacts [13, 14, 16–18]. Dual-energy CT is separated in detector- and tube-based methods. Four tube-based dual-energy techniques are available for clinical application; dual-source, dual-spin, split or twin beam, and kVp switching. The only available detector-based variant for clinical settings is the dual-layer spectral detector CT (SDCT). This system uses a dual-layer detector and a single x-ray source. Low-energetic photons are detected at the upper layer while high-energetic photons are detected at the lower layer [13, 16, 19].

Recently, the combination of MAR and VMI became possible. Both methods have already proved to be effective in reduction of artifacts from dental implants separately [5, 20] and have also shown advantages to one another for artifact reduction in other replacements [7, 9]. Therefore, the combination of these two techniques appears warranted. To the author's knowledge, this is the first study that investigates the combined use of VMI and MAR for artifact reduction in a subgroup of patients that suffers from strong metal artifacts from large dental implants and bridges, as compared to CI.

Materials and methods

This retrospective study was approved by the institutional review board and is in accordance with the ethical regulations of the 1964 Helsinki declaration as well as later amendments. Informed consent was waived. Inclusion criteria were (i) age, ≥ 18 years; (ii) contrast-enhanced staging examinations in portal-venous phase of the head and neck; (iii) large dental implants and bridges causing strong artifacts; and (iv) availability of MAR reconstructions in addition to conventional and spectral image reconstructions. MAR reconstructions were clinically only applied when strongest artifacts from large dental implants and bridges were present either strongly hampering diagnostic assessment or making it impossible. This resulted in the inclusion of 41 patients and examinations. Scanning was performed for clinical reasons only; no scan was conducted explicitly for the study.

Imaging protocol

All examinations were conducted on a clinical SDCT (IQon Spectral Detector CT, Philips Healthcare). Head-first supine position was used in all patients. Iodinated contrast media (Accupaque 350 mg/ml, GE Healthcare) was injected at a flow rate of 3.5 ml/s followed by a 30 ml saline flush intravenously. Acquisition was initialized with a 40-s delay after reaching a threshold value of 150 Hounsfield units (HU) in the descending aorta. Following scan parameters were applied: matrix 512 × 512, collimation 64 × 0.625 mm, rotation time 0.33 s, and pitch 1.296. Tube voltage was set to 120 kVp, and automatic tube current modulation was used in all examinations (DoseRight 3D-DOM, Philips Healthcare).

Reconstruction of conventional CT images (CI) and VMI ranging from 70 to 200 keV with an increment of 10 keV was carried out, applying a dedicated spectral reconstruction algorithm with a fixed soft tissue kernel (Spectral B, Philips Healthcare). CI reconstructed with the spectral algorithm

proved to be identical to CI reconstructions with vendor's hybrid iterative reconstruction algorithm regarding attenuation and image noise [21]. All images were reconstructed with a slice thickness of 1 mm in the axial plane. The proprietary image viewer (Intellispace Portal, Philips Healthcare) was used for all following analyses.

Objective analysis

Image assessment was carried out by a radiologist with 3 years of experience in oncologic imaging on axial image reconstructions using regions of interest (ROI) with a size set to 100 mm^2; however, ROI size was adaptively reduced to avoid inclusion of unrepresentative tissue. ROI placement was conducted in CI and MAR and transferred to VMI and VMI_{MAR} images thereafter. ROI were placed in most pronounced hypo- and hyperdense artifacts (slice selection was explicitly free to the readers' discretion to avoid any preselection bias). In addition, ROI were placed in a reference tissue without impairment by artifacts (e.g., when the hypodense artifact impaired muscle of the soft palate, reference tissue was muscle without impairment of artifacts). Further, ROI were placed in farther away soft tissue where artifacts were a little milder (mouth floor, soft palate) and in corresponding reference tissue without presence of artifacts (sternoclavicular muscle and subcutaneous fat). Attenuation (HU) and standard deviation (SD) were registered for all ROI. As in earlier studies, image noise was considered to be indicative of artifact burden [9, 20, 22]. The corrected image noise (CIN) as difference between image noise in artifact impaired soft tissue (mouth floor, soft palate), and corresponding non impaired reference tissue was calculated to correct for general lower image noise in high-keV reconstructions as recently suggested [12]. We also calculated the corrected attenuation (CA) as the difference between HU values in artifact impaired soft tissue (hypo- and hyperdense artifact, mouth floor/soft palate) and corresponding non-impaired reference tissue to adjust for changes in HU values that appear when changing VMI keV values (e.g., attenuation of muscles as well as arteries decreases and attenuation of fat increases with higher keV values).

Visual analysis

Visually, the extent of artifact reduction and diagnostic assessment of soft tissue (mouth floor, soft palate, and buccal soft tissue) was rated on 5-point Likert scales while the appearance of new artifacts was indicated on a tertiary scale by two radiologists with 2 and 3 years of experience in oncologic imaging, as described in Table 1. Additionally, both readers reported the optimal keV values for diagnostic assessment (artifact extent versus introduction of new artifacts and loss of soft tissue contrast).

The two readers further assessed the subjective image quality of CI, MAR, VMI, and VMI_{MAR}. For VMI and VMI_{MAR}, we chose reconstruction levels with greater increment (70 keV, 100 keV, 140 keV, and 200 keV) to allow for the detection of relevant changes and not to obscure differences by repetitive rating of too similar images. Following parameters were used: slice thickness 1 mm, axial plane, and soft tissue window settings. Further, readers were explicitly free to adjust window settings manually.

Statistical analysis

JMP software (JMP v12, SAS Institute) was used for statistical analyses. Quantitative results are displayed as mean (± standard deviation), and qualitative results are displayed by count and percentage. The Shapiro-Wilk test was applied to test for normal distribution. For further testing, the Wilcoxon test with steel adjustment for multiple comparisons was applied. Statistical significance was set to $p < 0.05$. The

Table 1 Visual analysis

Extent of hypo- and hyperdense artifacts	(5) Artifacts are absent/almost absent; (4) minor artifacts; (3) moderate artifacts, (2) pronounced artifacts; (1) massive artifacts
Diagnostic assessment of soft palate/mouth floor/-buccal soft tissue	(5) Fully diagnostic quality; (4) diagnostic interpretability is not affected by minor streaks; (3) minor artifacts only marginally affect the interpretability; (2) restricted diagnostic interpretability; (1) insufficient diagnostic interpretability by metal artifacts
Presence of new/unexpected artifacts as compared to CI	(3) No new/unexpected artifacts; (2) overcorrection of initial artifacts without impairment of diagnostic assessment as compared to CI; (1) new/unexpected artifacts with impairment of diagnostic assessment as compared to CI
Monoenergetic level with best diagnostic assessment (artifact extent versus introduction of new artifacts versus loss of soft tissue contrast)	

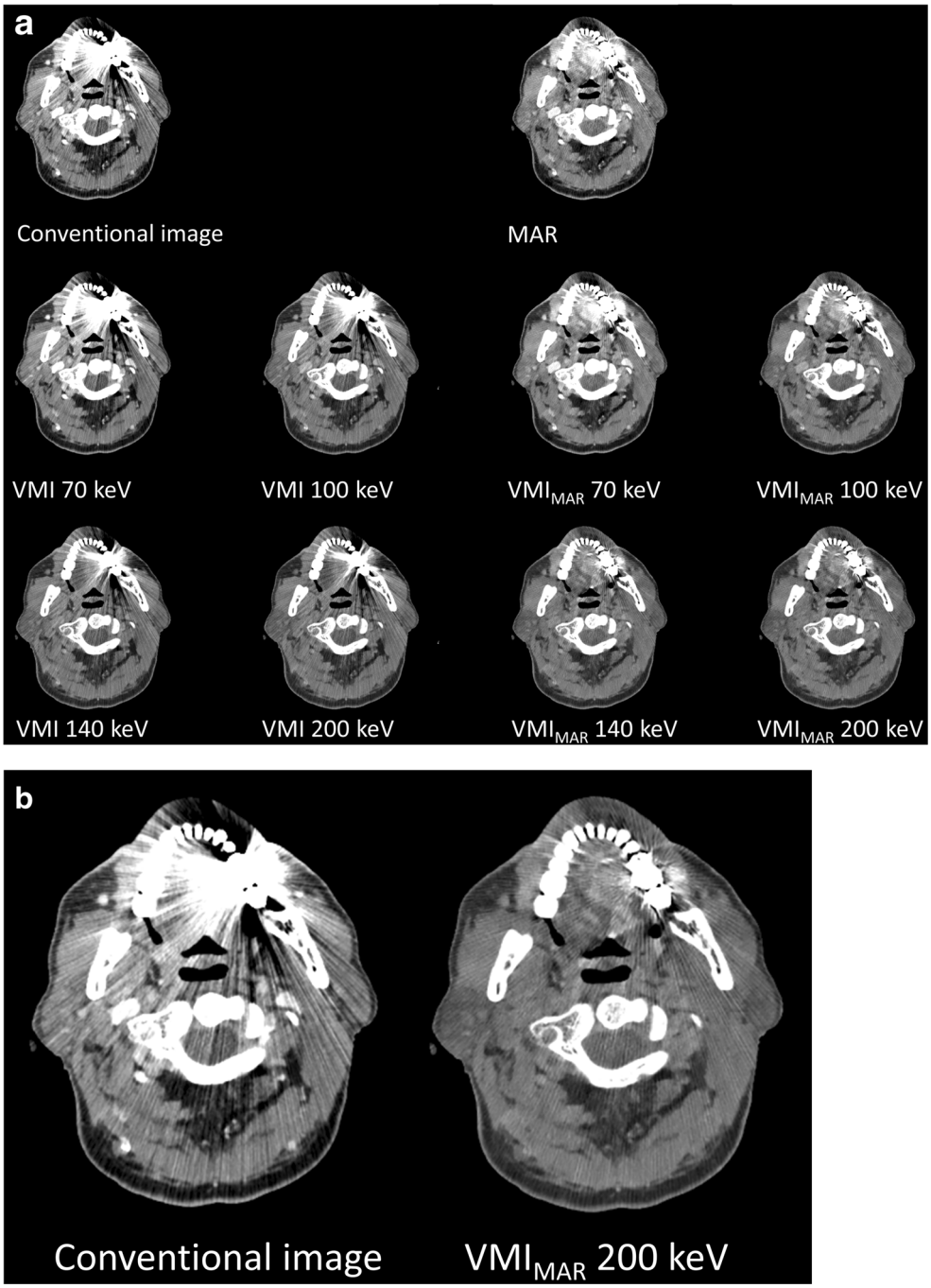

Fig. 1 Combination of MAR and VMI allows for an optimal reduction of strong artifacts impairing assessment of the mouth floor, soft palate and buccal soft tissue. **a** Axial planes in a patient with an implant in the left portion of the maxilla. Images were reconstructed as conventional (CI), metal artifact reduction algorithm (MAR), virtual monoenergetic images (VMI, 70 keV, 100 keV, 140 keV, and 200 keV), and the combination of MAR and VMI (VMI$_{MAR}$, 70 keV, 100 keV, 140 keV, and 200 keV; window center/width, 60/360 for all images). Visually, the best reduction is achieved by the combination of both methods at higher keV values, i.e., VMI$_{MAR}$ 140 keV and VMI$_{MAR}$ 200 keV images. MAR allows for the strongest artifact reduction. Higher keV VMI are especially effective in reducing hyperdense artifacts. **b** Enlargement of CI and VMI$_{MAR}$ at 200 keV

intraclass correlation coefficient (ICC) for visual analyses was assessed and interpreted as proposed earlier [23, 24].

Results

A total of 41 patients with an average age of 67.1 ± 11.9 years (range, 41–84 years) were included in the analysis. Among these, 13 were female and 28 male. Examined patients have been in an oncologic setting and were diseased with the following neoplasms: lymphoma $n = 16$, malignant melanoma $n = 11$, oral squamous cell carcinoma $n = 6$, gastric cancer $n = 4$, and others $n = 4$.

Objective assessment

Corrected attenuation, i.e., the difference between artifact impaired soft tissue and reference tissue, within the most pronounced/strong hypodense artifacts increased significantly with MAR and VMI$_{MAR}$ between 70 and 200 keV as compared

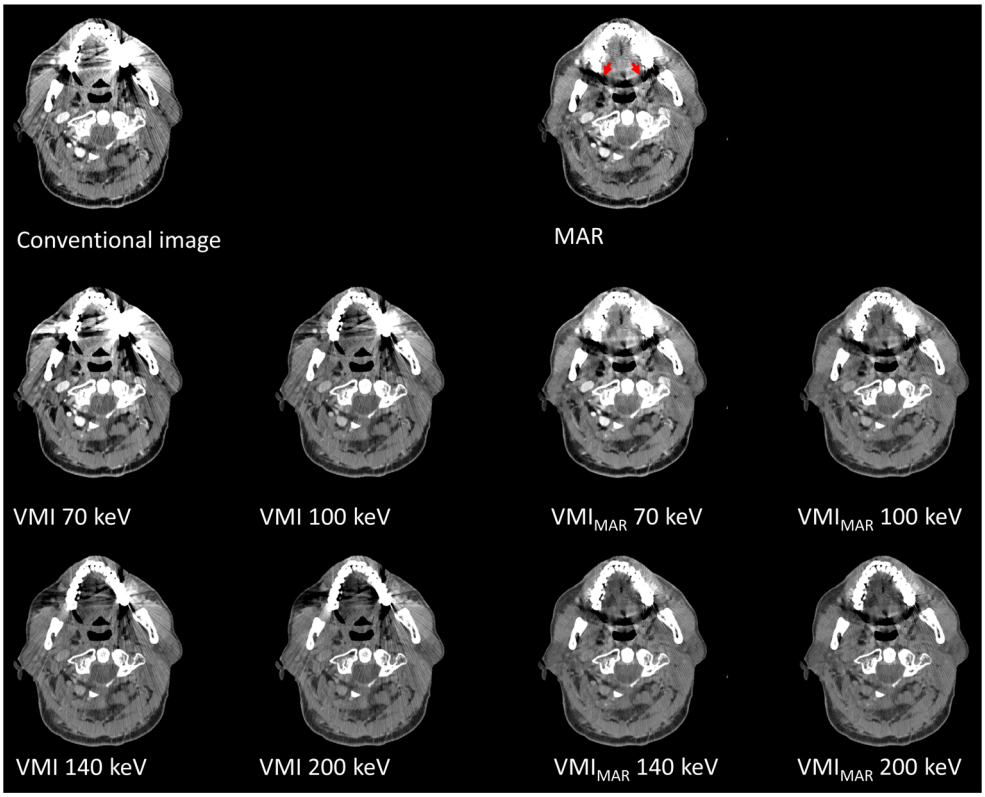

Fig. 2 Effective reduction of strong artifacts impairing assessment of the mouth floor, soft palate, and buccal soft tissue. Axial planes in a patient with an implant in the right and left portion of the maxilla. Images were reconstructed as conventional (CI), metal artifact reduction algorithm (MAR), virtual monoenergetic images (VMI, 70 keV, 100 keV, 140 keV, and 200 keV), and the combination of MAR and VMI (VMI$_{MAR}$, 70 keV, 100 keV, 140 keV and 200 keV; window center/width, 60/360 for all images). Visually, the best and almost complete reduction is achieved by the combination of both methods at higher keV values, i.e., VMI$_{MAR}$ 140 keV and VMI$_{MAR}$ 200 keV images. MAR allows for the strongest artifact reduction but also introduces new hypodense artifacts (red arrows). Higher keV VMI are especially effective in reducing hyperdense artifacts

to CI ($p < 0.001$, Figs. 1, 2, and 3, Table 2). On the other hand, MAR and VMI$_{MAR}$ led to a significant decrease of corrected attenuation values within the most pronounced/strong hyperdense artifacts, also corresponding to an approximation of their expected values (Figs. 1, 2, and 3, Table 2). In hyperdense artifacts, higher VMI and VMI$_{MAR}$ keV values led to an additional reduction of corrected attenuation values, thus approximating their true values; however, this tendency was not significant. In hypodense artifacts, higher keV values in VMI and VMI$_{MAR}$ did not allow for an (additional) reduction of artifacts (Fig. 3, Table 1).

Mouth floor and soft palate were affected by rather moderate hypodense artifacts. These hypodense artifacts were significantly reduced by MAR and VMI$_{MAR}$ as determined by corrected attenuation values. Higher keV values in VMI and VMI$_{MAR}$ did not allow for an additional artifact reduction (Fig. 4, Table 2). Corrected image noise, as the difference between artifact impaired soft tissue and not impaired reference tissue, represented by the standard deviation was found significantly lower in MAR and VMI$_{MAR}$. Higher keV values in VMI and VMI $_{MAR}$ also enabled additional reduction of image noise; however, this difference was not significant (Figs. 1, 2, and 4, Table 2).

Visual assessment

According to objective results reported above, subjectively hypodense and hyperdense artifacts were significantly reduced by MAR and VMI$_{MAR}$ at all keV values (Table 3). Higher keV values in VMI also led to a significant visual artifact reduction in hypodense artifacts at 200 keV VMI ($p < 0.05$). In line with the tendency of objective findings, higher keV VMI ($\geq$ 100 keV) was more effective for the reduction of subjective hyperdense artifacts. The diagnostic assessment of the mouth floor and soft palate was significantly improved using MAR and VMI$_{MAR}$ as compared to CI. In addition, VMI of $\geq$ 140 keV as compared to CI and VMI$_{MAR}$ of $\geq$ 100 keV as compared to MAR significantly improved diagnostic assessment. Optimal keV value for diagnostic assessment of surrounding soft tissues was 187.8 ± 28.1 keV (range, 100–200 keV) for VMI and 174.3 ± 36.7 keV (range, 70–200 keV) for VMI$_{MAR}$. Overcorrection of initial artifacts as compared to CI was noticed for VMI at 70 keV or higher (VMI at 70 keV 6%, at 100 keV 15%, at 140 keV 44%, and at 200 keV 50%), for MAR 22% and VMI$_{MAR}$ (VMI$_{MAR}$ at 70 keV 30%, at 100 keV 41%, at 140 keV 56%, and at 200 keV 57%). In addition, in a few patients, new artifacts were noted (VMI at 70 keV 0%, at 100 keV 0%, at 140 keV 7%, and at 200 keV 10%; MAR 4% and VMI$_{MAR}$ at 70 keV 4%, at 100 keV 4%, at 140 keV 4%, and at 200 keV 7%). Overall interrater agreement was excellent (ICC = 0.85); ICC values for each criterion are reported in Table 2.

Discussion

This study evaluated the reduction of strong artifacts from large dental implants and bridges in clinical routine comparing

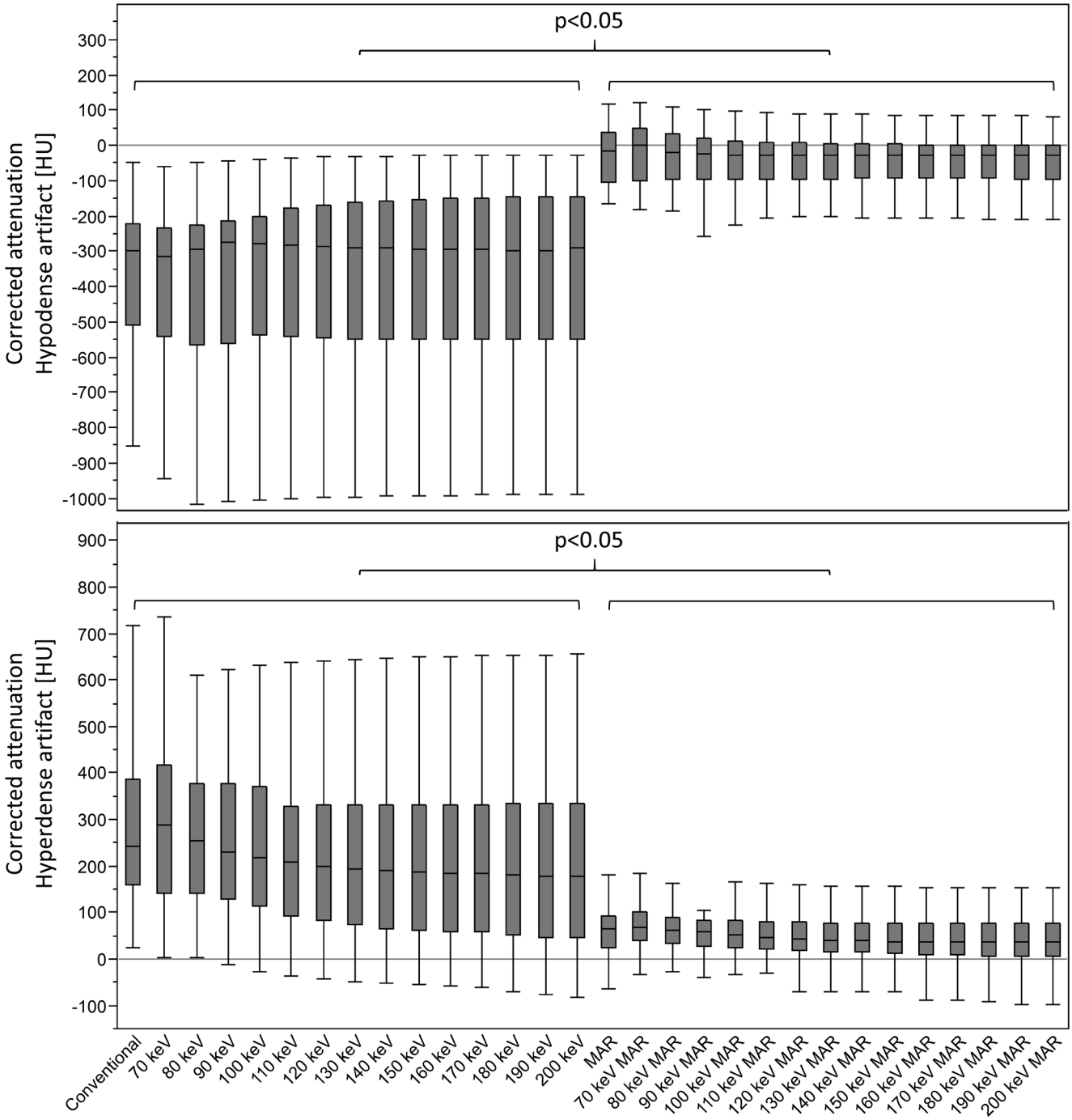

Fig. 3 Box-plot diagram displaying corrected attenuation values in hypo- and hyperdense artifacts due to large dental implants and bridges in conventional images (CI), virtual monoenergetic images, MAR, and combination of VMI and MAR (VMI/VMI_{MAR}, 70–200 keV). MAR and VMI_{MAR} allow for a significant artifact reduction as compared to CI. Higher keV values for VMI and VMI_{MAR} offer an additional reduction of hyperdense artifacts; however, this trend was not statistically significant

conventional CT images to VMI, MAR, and their combination. MAR and VMI_{MAR} showed strong and significant reduction of both hypodense and hyperdense artifacts as well as image noise. This also resulted in improved diagnostic assessment of the mouth floor and soft palate. The improved depiction and diagnostic assessment of the head and neck might also allow for higher diagnostic certainties pertaining to the detection of pathologies, such as soft tissue metastases, inflammation, and traumatic injuries.

Dedicated metal artifact reduction algorithms became available during the past years exploiting increased computational power for image reconstruction [7, 25]. Besides reducing artifacts from various kinds of orthopedic hardware, e.g., arthroplasties of the hip, spinal fusions, and

Table 2 Objective assessment of artifact reduction and surrounding tissue

	Corrected attenuation			Corrected image noise
	Hypodense artifact	Hyperdense artifact	Artifact impaired soft tissue	Artifact impaired soft tissue
CI	(−)369.8 ± 239.6	274.8 ± 170.2	(−)92.5 ± 121.9	30.6 ± 26.4
VMI				
70 keV	(−)391.2 ± 248.1	296.0 ± 207.5	(−)99.7 ± 135.4	28.2 ± 25.6
100 keV	(−)383.1 ± 257.3	250.3 ± 191.9	(−)81.3 ± 108.4	28.4 ± 26.9
140 keV	(−)379.1 ± 270.5	232.1 ± 206.0	(−)73.9 ± 108.9	29.1 ± 27.7
200 keV	(−)377.2 ± 277.9	223.9 ± 214.6	(−)70.6 ± 111.5	29.6 ± 28.1
MAR	*(−)37.3 ± 109.6*	*51.3 ± 150.8*	*(−)26.4 ± 57.0*	*14.3 ± 16.2*
VMI-MAR				
70 keV	*(−)31.5 ± 99.0*	*62.7 ± 60.0*	*(−)27.9 ± 60.9*	*13.5 ± 16.6*
100 keV	*(−)40.8 ± 77.3*	*46.2 ± 54.3*	*(−)28.9 ± 53.3*	*13.1 ± 14.5*
140 keV	*(−)44.5 ± 72.4*	*39.6 ± 55.0*	*(−)29.3 ± 52.0*	*13.1 ± 13.9*
200 keV	*(−)46.2 ± 71.0*	*36.6 ± 56.0*	*(−)29.5 ± 51.8*	*13.1 ± 13.7*
p values				
CI vs. VMI 70 keV	$p > 0.05$	$p > 0.05$	$p > 0.05$	$p > 0.05$
CI vs. VMI 100 keV	$p > 0.05$	$p > 0.05$	$p > 0.05$	$p > 0.05$
CI vs. VMI 140 keV	$p > 0.05$	$p > 0.05$	$p > 0.05$	$p > 0.05$
CI vs. VMI 200 keV	$p > 0.05$	$p > 0.05$	$p > 0.05$	$p > 0.05$
CI vs. MAR	$p < 0.001$	$p < 0.001$	$p = 0.007$	$p < 0.05$
CI vs. VMI-MAR 70–200 keV	$p < 0.001$	$p < 0.001$	$p < 0.05$	$p < 0.05$

Corrected attenuation, corrected attenuation/HU values; Corrected image noise, corrected image noise/standard deviation; *CI*, conventional images; *VMI*, virtual monoenergetic images; *MAR*, metal artifact reduction algorithms; *VMI-MAR*, combination of virtual monoenergetic images and metal artifact reduction algorithms; Artifact impaired soft tissue, mouth floor and soft palate. Significant changes in HU values as compared to CI are marked in italics ($p < 0.05$)

peripheral plates, and screws, the specific algorithm used in this study was proven to successfully reduce artifacts from smaller hardware such as dental implants and deep brain stimulation leads [5, 7, 20]. Similar algorithms are available from all major vendors. The unique aspect of the MAR algorithm lies in the first step, in which a pre-segmentation of image information is performed. In the course of this, all pixels containing non-metal information are set to zero, resulting in a metal-only image which then undergoes forward projection enabling to identify sonogram regions containing metal artifacts. However, as certain thresholds have to be met in this first step, the algorithm does not manipulate images without or very little metal present, while it especially addresses hypodense artifacts from large orthopedic implants. Further details on the algorithm have been reported earlier [6, 7].

Another powerful tool for artifact reduction are virtual monoenergetic images obtained from dual-energy CT. Irrespective of the specific technology and/or vendor, high-keV images did demonstrate an impressive capability for artifact reduction in artifacts occurring due to a variety of different metal implants [10, 26–31]. As opposed to MAR, VMI should theoretically be particularly powerful in reducing hyperdense streaks which was confirmed by several recent publications [4, 9, 32].

The combination of both techniques (MAR and VMI) is challenging if image processing cannot integrate all available information in the projection domain which is the case for all emission-based dual-energy CT systems. In SDCT on the other hand, high and low energy information is obtained matched in terms of temporal and spatial resolution; therefore, combining VMI with MAR processing is facilitated. Recent studies evaluated their combination in presence of arthroplasties of the hip and deep brain stimulation electrodes. They reported that both techniques rather supplement each other than demonstrating clear superiority [7, 9].

In context of dental implants and crowns in imaging of head and neck, both techniques separately have proven utility while their combination has not been evaluated [5, 20]. A recent study used VMI derived from SDCT for metal artifact reduction of dental implants, reporting that VMI with increasing keV lead to a significant reduction of metal artifacts [20]. As opposed to their findings, we did not find a significant artifact reduction in VMI. This might be well explained by

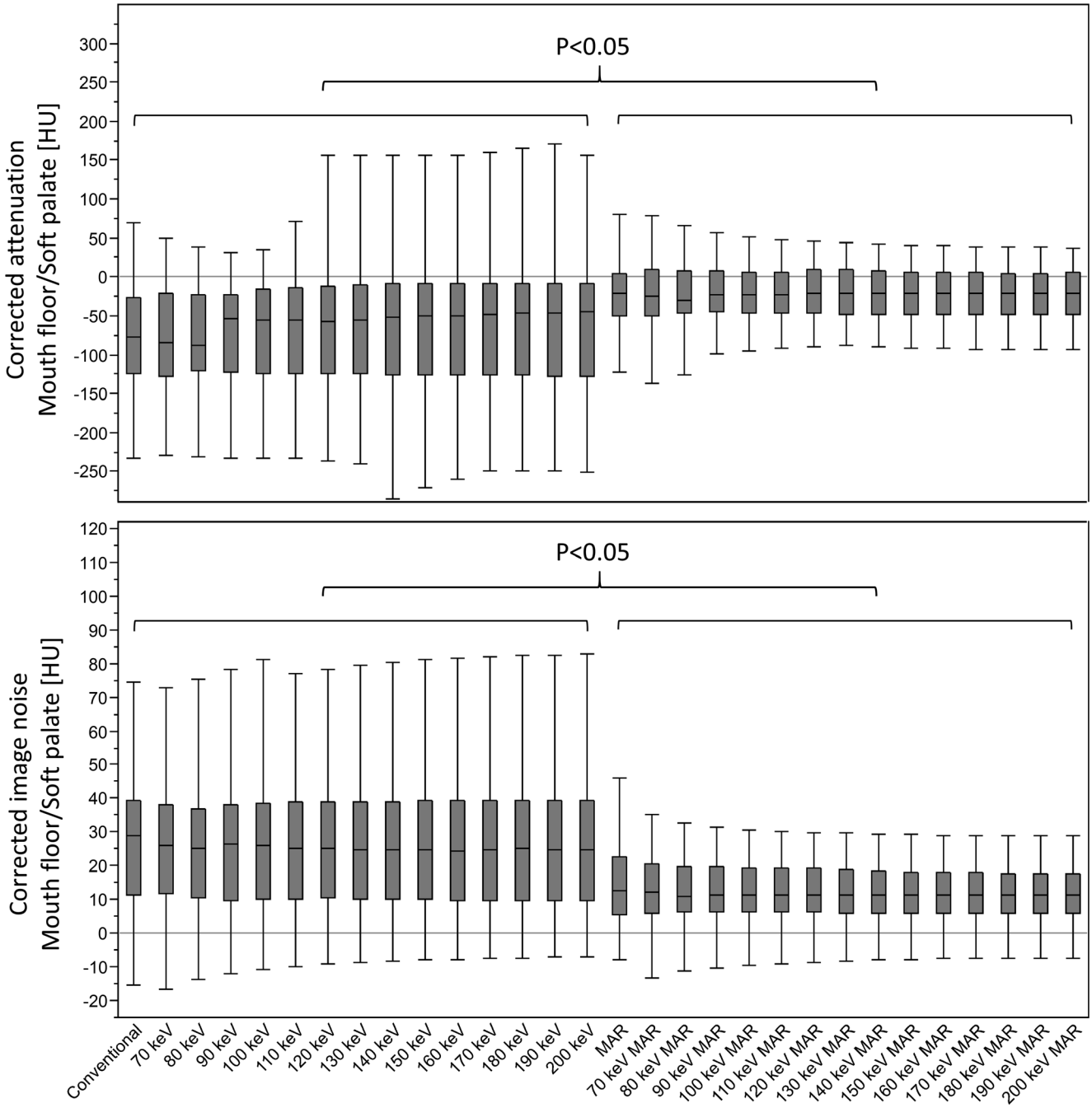

Fig. 4 Box-plot diagram displaying corrected attenuation and corrected image in artifact impaired soft tissue (mouth floor and soft palate) in conventional images (CI), virtual monoenergetic images, MAR, and combination of VMI and MAR (VMI/VMI_{MAR}, 70–200 keV). MAR and VMI_{MAR} allow for a significant artifact reduction as compared to CI regarding corrected attenuation as well as corrected image noise

the fact that we only included exams for which MAR reconstructions were available, which constitutes a selection bias towards strong artifacts. VMI especially failed to reduce hypodense streaks, which in turn is a strength of MAR. In the presence of strong artifacts, the utility of MAR is more powerful than VMI, but should be combined with VMI if available.

One issue with either approach that has been reported earlier and was also present in our study is the introduction of new artifacts [5, 8, 9, 20, 33]. For VMI, these new artifacts mostly occurred in the location of the artifacts also seen in CI and were interpreted as an overcorrection, as they did not impair diagnostic assessment [20]. MAR introduced image distortion and blurring which were, in most cases, slight and did not hamper image interpretation [5, 9]. In very few cases only, VMI and MAR introduced new artifacts that impaired diagnostic assessment as compared to CI. Therefore, VMI, MAR, and VMI_{MAR} could be used as supplemental image

Table 3 Subjective assessment of artifact reduction and surrounding soft tissue

	Artifact extent			New artifacts
	Hypodense	Hyperdense	Soft tissue	
CI	2 (1–3)	1 (1–2)	1 (1–2)	
VMI				
70 keV	2 (1–3)	1 (1–2)	1 (1–2)	3 (2–3)
100 keV	2 (1–3)	*1 (1–2)*	1 (1–2)	3 (2–3)
140 keV	2 (1–3)	*2 (2–3)*	*1 (1–3)*	3 (2–3)
200 keV	*2 (1–3)*	*2 (2–3)*	*2 (1–3)*	2.5 (1–3)
MAR	*3.5 (2–4)*	*2 (1–3)*	*2 (1–3)*	3 (2–3)
VMI-MAR				
70 keV	*4 (2–4)*	*3 (2–3)*	*2 (2–3)*	3 (2–3)
100 keV	*4 (2–4)*	*3 (2–4)*	*2.5 (2–4)*	3 (2–3)
140 keV	*3 (2–4)*	*3 (2–4)*	*3 (2–4)*	2 (1–3)
200 keV	*3 (2–4)*	*3 (3–5)*	*3 (2–4)*	2 (1–3)
ICC	0.81	0.88	0.87	0.66
p values				
CI vs. VMI 70 keV	$p > 0.05$	$p > 0.05$	$p > 0.05$	
CI vs. VMI 100 keV	$p > 0.05$	$p < 0.001$	$p > 0.05$	
CI vs. VMI 140 keV	$p > 0.05$	$p < 0.001$	$p = 0.024$	
CI vs. VMI 200 keV	$p = 0.025$	$p < 0.001$	$p < 0.001$	
CI vs. MAR	$p < 0.001$	$p < 0.001$	$p < 0.001$	
CI vs. VMI-MAR 70–200 keV	$p < 0.001$	$p < 0.001$	$p < 0.001$	
MAR vs. VMI-MAR 70 keV	$p > 0.05$	$p = 0.035$	$p > 0.05$	
MAR vs. VMI-MAR 100 keV	$p > 0.05$	$p < 0.001$	$p < 0.001$	
MAR vs. VMI-MAR 140 keV	$p > 0.05$	$p < 0.001$	$p < 0.001$	
MAR vs. VMI-MAR 200 keV	$p > 0.05$	$p < 0.001$	$p < 0.001$	

Vessels, axillary and subclavian vessels; Soft tissue, adjacent soft tissue (mouth floor, soft palate, and buccal soft tissue); overcorrection/new artifacts as compared to conventional images; *ICC*, intraclass correlation coefficient; *CI*, conventional images; *VMI*, virtual monoenergetic images; *MAR*, metal artifact reduction algorithms; *VMI-MAR*, combination of virtual monoenergetic images and metal artifact reduction algorithms. Data is reported as median and 10/90% quantile. Significant changes in HU values as compared to CI are marked in italics ($p < 0.05$)

information in addition to CI which remains the standard of care. Artifact reduction at higher keV levels is stronger while there is also a greater risk of introducing overcorrection and new artifacts; therefore, optimal keV values for diagnostic assessment need to be carefully adjusted and possibly adapted to the specific patient and/or implant. This underlines the need for the possibility of real-time adjustment. In addition, there are numerous reports indicating a dependency on material alloy for effectiveness of MAR, VMI, and VMI_{MAR}; future studies are encouraged to assess this further.

The following limitations should be considered: We only included patients that received an additional MAR reconstruction due to strong artifacts; therefore, our study has a selection bias. This might also explain why VMI at higher keV values were not as effective as reported in earlier studies [20, 34] as they might fail in strong metal artifacts [7, 9, 35]. Further, various kinds of oral implants with different compositions of metal alloys were examined. The composition can impact shape and severity of the corresponding metal artifacts as well as possibly also the efficiency of MAR and VMI for their reduction. Unfortunately, more detailed information on the kind of oral implant were not available in our study cohort. We included contrast-enhanced CT examinations only as we feel that these examinations benefit the most from artifact reduction in proximity to the oral cavity, and the standardized protocol allowed us to systematically demonstrate our findings in a larger patient cohort. The high-keV images will result in a loss of image contrast, especially of iodine-associated attenuation as distance to k-edge increases [16]. Unenhanced CT scans should be less susceptible to this effect; however, a slight loss in soft tissue contrast is expected to occur in these images as well. Several approaches have been applied to measure artifacts in CT imaging. Measuring HU values or artifact widths are common methods for determination of artifacts but also more complex techniques have been used, such as dedicated algorithms within either projection or image domain that

allow for artifact quantification [9, 20, 22, 26, 27, 36]. Image noise can be considered as indicative for presence of artifacts; however, as there are general changes in attenuation and image noise with higher VMI keV values, we applied an intra individual comparison between tissue impaired by artifacts and correspondent reference tissue without impairment of artifacts, i.e., corrected image noise and corrected attenuation [16, 20]. Iterative reconstructions themselves also have a strong impact on image noise. Therefore, they may decrease the meaningfulness of the used method. For possible limitations in the objective analyses, a detailed subjective analysis by two independent and experienced readers was conducted. They assessed artifact reduction and diagnostic assessment. Clear results and high interreader agreement indicate validity of their assessment.

To conclude, we found that in the presence of strong artifacts due to large oral implants, especially MAR is a powerful mean for artifact reduction. In light of such strong artifacts, the benefit from VMI can be partly limited. Nevertheless, in hyperdense artifacts, MAR are supplemented by VMI acquired from SDCT ranging from 140 to 200 keV, which is why we suggest combining both techniques in order to attain the best possible artifact reduction and to improve diagnostic image assessment in imaging of the head and neck.

Funding The authors state that this work has not received any funding.

Compliance with ethical standards

Guarantor The scientific guarantor of this publication is Kai Roman Laukamp.

Conflict of interest The authors of this manuscript declare relationships with the following companies: David Maintz, Jan Borggrefe, and Nils Große Hokamp received speakers' honoraria from Philips Healthcare.

Statistics and biometry No complex statistical methods were necessary for this paper.

Informed consent Written informed consent was waived by the Institutional Review Board.

Ethical approval Institutional Review Board approval was obtained.

Methodology
- retrospective
- experimental
- performed at one institution

References

1. Fayad LM, Patra A, Fishman EK (2009) Value of 3D CT in defining skeletal complications of orthopedic hardware in the postoperative patient. AJR Am J Roentgenol 193:1155–1163
2. Lee MJ, Kim S, Lee SA et al (2007) Overcoming artifacts from metallic orthopedic implants at high-field-strength MR imaging and multi-detector CT. Radiographics 27:791–803
3. Mori I, Machida Y, Osanai M, Iinuma K (2013) Photon starvation artifacts of X-ray CT: their true cause and a solution. Radiol Phys Technol 6:130–141
4. Boas FE, Fleischmann D (2012) CT artifacts: causes and reduction techniques. Imaging Med 4:229–240
5. Kidoh M, Nakaura T, Nakamura S et al (2014) Reduction of dental metallic artefacts in CT: value of a newly developed algorithm for metal artefact reduction (O-MAR). Clin Radiol 69:e11–e16
6. Philips CT Clinical Science (2012) Metal Artifact Reduction for Orthopedic Implants (O-MAR) [Philips NetForum Community]. Jan 8, 2012. Available at: http://clinical.netforum.healthcare.philips.com/us_en/Explore/White-Papers/CT/Metal-Artifact-Reduction-for-Orthopedic-Implants-(O-MAR). Accessed 1 Jul 2017
7. Große Hokamp N, Hellerbach A, Gierich A et al (2018) Reduction of artifacts caused by deep brain stimulating electrodes in cranial computed tomography imaging by means of virtual monoenergetic images, metal artifact reduction algorithms, and their combination. Invest Radiol 53:421–431
8. Huang JY, Kerns JR, Nute JL et al (2015) An evaluation of three commercially available metal artifact reduction methods for CT imaging. Phys Med Biol 60:1047–1067
9. Laukamp KR, Lennartz S, Neuhaus VF et al (2018) CT metal artifacts in patients with total hip replacements: for artifact reduction monoenergetic reconstructions and post-processing algorithms are both efficient but not similar. Eur Radiol 28(11)4524–4533
10. Boomsma MF, Warringa N, Edens MA et al (2016) Quantitative analysis of orthopedic metal artefact reduction in 64-slice computed tomography scans in large head metal-on-metal total hip replacement, a phantom study. Springerplus 5:405
11. Bolstad K, Flatabø S, Aadnevik D, Dalehaug I, Vetti N (2018) Metal artifact reduction in CT, a phantom study: subjective and objective evaluation of four commercial metal artifact reduction algorithms when used on three different orthopedic metal implants. Acta Radiol 59(9):1110–1118
12. Große Hokamp N, Neuhaus V, Abdullayev N et al (2017) Reduction of artifacts caused by orthopedic hardware in the spine in spectral detector CT examinations using virtual monoenergetic image reconstructions and metal-artifact-reduction algorithms. Skeletal Radiol 47(2):195–201
13. Flohr TG, McCollough CH, Bruder H et al (2006) First performance evaluation of a dual-source CT (DSCT) system. Eur Radiol 16:256–268
14. Lewis M, Reid K, Toms AP (2013) Reducing the effects of metal artefact using high keV monoenergetic reconstruction of dual energy CT (DECT) in hip replacements. Skelet Radiol 42:275–282
15. Wellenberg RH, Boomsma MF, van Osch JA et al (2017) Quantifying metal artefact reduction using virtual monochromatic dual-layer detector spectral CT imaging in unilateral and bilateral total hip prostheses. Eur J Radiol 88:61–70
16. McCollough CH, Leng S, Yu L, Fletcher JG (2015) Dual- and multi-energy CT: principles, technical approaches, and clinical applications. Radiology 276:637–653
17. Johnson TR (2012) Dual-energy CT: general principles. AJR Am J Roentgenol 199:S3–S8
18. Alvarez RE, Macovski A (1976) Energy-selective reconstructions in X-ray computerized tomography. Phys Med Biol 21:733–744
19. Silva AC, Morse BG, Hara AK, Paden RG, Hongo N, Pavlicek W (2011) Dual-energy (spectral) CT: applications in abdominal imaging. Radiographics 31:1031–1046
20. Große Hokamp N, Laukamp KR, Lennartz S et al (2018) Artifact reduction from dental implants using virtual monoenergetic reconstructions from novel spectral detector CT. Eur J Radiol 104:136–142

21. Große Hokamp N, Höink AJ, Doerner J et al (2017) Assessment of arterially hyper-enhancing liver lesions using virtual monoenergetic images from spectral detector CT: phantom and patient experience. Abdom Radiol (NY) 43(8):2066–2074
22. Bamberg F, Dierks A, Nikolaou K, Reiser MF, Becker CR, Johnson TR (2011) Metal artifact reduction by dual energy computed tomography using monoenergetic extrapolation. Eur Radiol 21: 1424–1429
23. Cohen J (1960) A coefficient of agreement for nominal scales. Educ Psychol Meas 20:37–46
24. Fleiss JL, Cohen J (1973) The equivalence of weighted kappa and the intraclass correlation coefficient as measures of reliability. Educ Psychol Meas 33:613–619
25. Willemink MJ, De Jong PA, Leiner T et al (2013) Iterative reconstruction techniques for computed tomography part 1: technical principles. Eur Radiol 23:1623–1631
26. Aissa J, Thomas C, Sawicki LM et al (2017) Iterative metal artefact reduction in CT: can dedicated algorithms improve image quality after spinal instrumentation? Clin Radiol 72:428.e7–428.e12
27. Mangold S, Gatidis S, Luz O et al (2014) Single-source dual-energy computed tomography: use of monoenergetic extrapolation for a reduction of metal artifacts. Invest Radiol 49:788–793
28. Lee YH, Park KK, Song HT, Kim S, Suh JS (2012) Metal artefact reduction in gemstone spectral imaging dual-energy CT with and without metal artefact reduction software. Eur Radiol 22:1331–1340
29. Dong Y, Shi AJ, Wu JL et al (2016) Metal artifact reduction using virtual monochromatic images for patients with pedicle screws implants on CT. Eur Spine J 25:1754–1763
30. Albrecht MH, Trommer J, Wichmann JL et al (2016) Comprehensive comparison of virtual monoenergetic and linearly blended reconstruction techniques in third-generation dual-source dual-energy computed tomography angiography of the thorax and abdomen. Invest Radiol 51:582–590
31. Guggenberger R, Winklhofer S, Osterhoff G et al (2012) Metallic artefact reduction with monoenergetic dual-energy CT: systematic ex vivo evaluation of posterior spinal fusion implants from various vendors and different spine levels. Eur Radiol 22:2357–2364
32. Kalisz K, Buethe J, Saboo SS, Abbara S, Halliburton S, Rajiah P (2016) Artifacts at cardiac CT: physics and solutions. Radiographics 36:2064–2083
33. Kuchenbecker S, Faby S, Sawall S, Lell M, Kachelrieß M (2015) Dual energy CT: how well can pseudo-monochromatic imaging reduce metal artifacts? Med Phys 42:1023–1036
34. Cha J, Kim HJ, Kim ST, Kim YK, Kim HY, Park GM (2017) Dual-energy CT with virtual monochromatic images and metal artifact reduction software for reducing metallic dental artifacts. Acta Radiol 58:1312–1319
35. Neuhaus V, Große Hokamp N, Abdullayev N et al (2017) Metal artifact reduction by dual-layer computed tomography using virtual monoenergetic images. Eur J Radiol 93:143–148
36. Bongers MN, Schabel C, Thomas C et al (2015) Comparison and combination of dual-energy- and iterative-based metal artefact reduction on hip prosthesis and dental implants. PLoS One 10: e0143584